Reliable anisotropic-adaptive discontinuous Galerkin method for simplified $\mathbf{P_N}$ approximations of radiative transfer

Stefano Giani

Department of Engineering, Durham University, Lower Mountjoy, South Road, Durham, DH1 3LE, United Kingdom, stefano.giani@durham.ac.uk

Abstract

In this paper we present the analysis for the error estimator for radiative transfer problems presented in [1] where we showed the capabilities of the error estimator to accurately drive the adaptivity to resolve steep boundary layers, which are among the difficulties that most numerical methods fail to resolve accurately. We prove reliability for the error estimator in terms of a global upper bound of the error measured in the natural norm. We present a series of numerical experiments to test the efficiency of this approach within a fully automated *hp*-adaptive refinement algorithm.

Keywords: discontinuous Galerkin, anisotropic adaptivity, radiative transfer, error estimator
2000 MSC: 65N30, 65N15, 65N50, 82D20

1. Introduction

In the current work, we consider the simplified $\mathrm{P_N}$ (SP_N) approximations to the radiative transfer equations. Such approximations were first proposed in [2] and theoretically studied in [3], the main advantage of these approximations, compared to the full radiative transfer equation, is the fact that the radiative transfer equations are transformed to a mixed set of elliptic equations independent of the angular directions. The accuracy of the models have been studied extensively already, see [4, 5, 6, 7]. An unavoidable characteristic of the SP_N approximations are boundary layers appears in the solutions, which are in general difficult to resolve numerically. In order to deal with that, we propose to use anisotropic mesh adaptivity capable of creating automatically anisotropic elements along the boundary aligned with the boundary layers. This is done automatically thanks to our error estimator that can successfully detect and resolve the difficult features of the solutions, delivering very accurate results with a moderate computational cost.

In the current study we derive a posteriori error estimates for the DG discretization of $\mathrm{SP_N}$ approximations and we prove the reliability of the a posteriori error estimator. In practise, this is a very useful result because in general the true approximation error is unknown, since the exact solution of the problem is not known, see [1] for few examples where the error estimator is applied to problems with solutions that are not known analytically. However,

the error estimator is always computable and it gives an estimation of the true error making possible to judge if the accuracy of the computed solution is enough. The error estimator used in this work is a modification of the error estimator for convection-diffusion problems presented in [8]. The error estimator is tested extensively in [1] on challenging radiative transfer problems, therefore in the present work we focus on the analysis and the numerical efficiency of the method.

Discontinuous Galerkin (DG) methods are becoming very important tools to compute numerical approximation of PDEs [9, 8, 10, 11, 12, 13, 14] due to their flexibility in applying high order discretization, in treating hanging nodes and particularly in the contest of this paper in allowing for very anisotropic elements. The flexibility of DG methods makes them ideal for *hp*-adaptivity, in which both the size and shape of the elements (*h*-adaptivity) and their polynomial orders (*p*-adaptivity) are adjusted to improve the accuracy of the solution.

There is a great amount of literature on standard continuous finite element methods using anisotropic elements; see e.g., [15, 16, 17, 18] and the references therein. There are also some works on anisotropic meshes considering Discontinuous Galerkin (DG) methods; see e.g., [19, 20, 21] and the references therein. However to our knowledge this is the first time that the analysis for an error estimator on anisotropic meshes for radiative transfer problems is presented. This is surprisingly in view of the fact boundary layers are very common for such problem.

The outline of the rest of this paper is as follows. In Section 2, we introduce *hp*-adaptive discontinuous Galerkin methods for the SP_1 and SP_3 approximations. In Section 3, we present the error estimator and the reliability result. In Section 4, we present a series of numerical tests that illustrate the theoretical results. Finally, in Section 5, we end with concluding remarks.

2. Interior penalty discretization

In this section we introduce our DG method for solving the SP_1 and SP_3 approximations, see [1] for the derivation of the approximations. The SP_N approximations can be rearranged in a compact form as

$$\begin{aligned} -\nabla\cdot(A\nabla\phi)+B\phi &= F, \\ C\mathbf{n}(\hat{\mathbf{x}})\cdot\nabla\phi+D\phi &= G, \end{aligned} \tag{1}$$

where the variables in the compact form (1) for the SP_1 approximation are defined as

$$\phi=\varphi,\quad A=\frac{\varepsilon^2}{3\,(\kappa+\sigma)},\quad B=\kappa,\quad C=\frac{1+3r_2}{1-2r_1}\frac{2\varepsilon}{3\,(\kappa+\sigma)},\quad D=1,$$

where ϵ is the optical thickness coefficient, κ the absorption coefficient, σ the scattering coefficient and the parameters r_1 and r_2 express the reflectivity of the considered media. For the SP_1 approximation F and G are the data in the interior of the domain and along the

boundary. For the SP_3 approximation we have

$$\phi = \begin{pmatrix} \psi_1 \\ \psi_2 \end{pmatrix}, \quad A = \begin{pmatrix} \dfrac{\varepsilon^2 \mu_1^2}{\kappa + \sigma} & 0 \\ 0 & \dfrac{\varepsilon^2 \mu_2^2}{\kappa + \sigma} \end{pmatrix},$$

$$B = \begin{pmatrix} \kappa \\ \kappa \end{pmatrix}, \quad C = \begin{pmatrix} \dfrac{\varepsilon}{\kappa + \sigma} \\ \dfrac{\varepsilon}{\kappa + \sigma} \end{pmatrix}, \quad D = \begin{pmatrix} \alpha_1 & \beta_2 \\ \beta_1 & \alpha_2 \end{pmatrix},$$

where the parameters μ_i, α_i and β_i $(i = 1, 2)$ are derived using asymptotic and variational analyses, see reference [4]. In the SP_3 approximation, F and G are vector-valued functions of dimension two. It is interesting to notice that in the SP_3 approximation the two equations are only coupled through the Robin boundary condition. We assume that all constants involved in problem (1) are non-negative and bounded on Ω and we assume that the variation of each constant is not too large in the sense that the ratio of the maximum and minimum values is not large.

2.1. Anisotropic meshes

Any mesh ζ used in this work is a subdivision of Ω, with K denoting a generic element. We assume that the subdivision ζ is constructed via affine mappings $F_K : \hat{K} \longrightarrow K$ where $\hat{K}$ is the reference square. We allow for a maximum of one hanging node per edge and we denote $\mathcal{E}(\zeta)$ and $\mathcal{E}^{int}(\zeta) \subset \mathcal{E}(\zeta)$ the set of all edges of the mesh ζ and the subset of all interior edges respectively and by $\mathcal{E}^{BC}(\zeta) \subset \mathcal{E}(\zeta)$ the subset of all boundary edges. To allow for anisotropic elements, we define the two anisotropic vectors $\underline{\mathrm{v}}_K^1$ and $\underline{\mathrm{v}}_K^2$, see Figure 1a. These vectors reflect the two anisotropic directions of the generic element K and their lengths are denoted by h_K^1 and h_K^2, respectively. Thus,

$$h_K^1 = \text{length}\left(\underline{\mathrm{v}}_K^1\right), \qquad h_K^2 = \text{length}\left(\underline{\mathrm{v}}_K^2\right).$$

We also set

$$h_{\min,K} = \min\left(h_K^1, h_K^2\right), \qquad h_{\max,K} = \max\left(h_K^1, h_K^2\right).$$

Let $\mathbf{M}_K$ denote the matrix formed by the anisotropic vectors $\underline{\mathrm{v}}_K^1$ and $\underline{\mathrm{v}}_K^2$ as

$$\mathbf{M}_K = \left(\underline{\mathrm{v}}_K^1, \underline{\mathrm{v}}_K^2\right). \tag{2}$$

Moreover the matrix $\mathbf{M}_K$ satisfies

$$\mathbf{M}_K^\top \mathbf{M}_K = \begin{pmatrix} (h_K^1)^2 & 0 \\ 0 & (h_K^2)^2 \end{pmatrix}.$$

Given an edge $E \in \mathcal{E}(\zeta)$, for any element $K \in \zeta$, if $E \in \mathcal{E}(K)$, we define a local function of the edge E as

$$\mathrm{h}_{E,K}^{\perp} = h_K^{3-i}, \qquad \text{if } E \text{ is parallel to } \underline{\mathrm{v}}_K^i, \quad i = 1, 2.$$

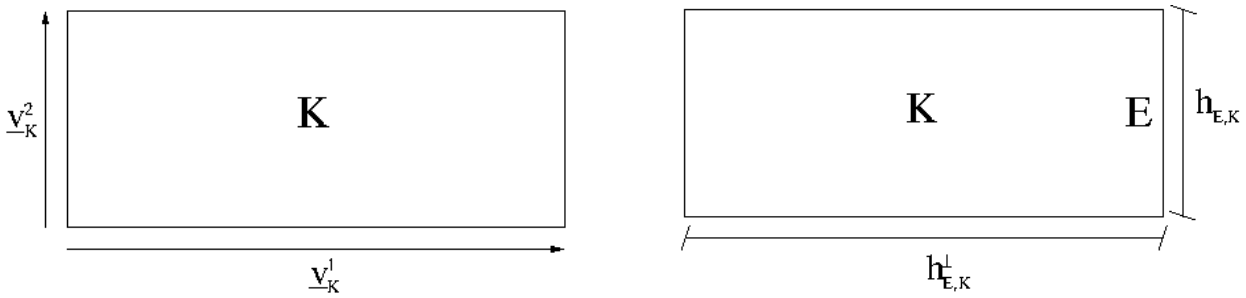

(a) (b)

Figure 1: (a) General element K with anisotropic vectors $\underline{\mathrm{v}}_K^i$, $i = 1, 2$ describing the anisotropicity of the element. (b) General edge E of element K with corresponding definitions of $\mathrm{h}_{E,K}$ and $\mathrm{h}_{E,K}^{\perp}$.

Moreover, for any $E \in \mathcal{E}^{int}(\zeta)$, we assume that

$$\mathrm{h}_{E,K}^{\perp} \sim \mathrm{h}_{E,K'}^{\perp}, \qquad E = K \cap K', \quad K, K' \in \zeta. \tag{3}$$

In order to clarify the definitions of $\mathrm{h}_{E,K}$ and $\mathrm{h}_{E,K}^{\perp}$, in Figure 1b the length of $\mathrm{h}_{E,K}$ and $\mathrm{h}_{E,K}^{\perp}$ are reported for a general edge E in a general element K. Notice that the assumption (3) does not bound the aspect ratios of elements. For any edges $E, E' \in \mathcal{E}(K)$ and $E \cap E' \neq \emptyset$, $h_E/h_{E'}$ can be significantly large. If $E \in \mathcal{E}(K)$ is parallel to $\underline{\mathrm{v}}_K^i$, $i = 1, 2$, we define

$$h_{E,K} = h_K^i, \qquad i = 1, 2.$$

For any edge $E \in \mathcal{E}(\zeta)$, we further set

$$\mathrm{h}_E^{\perp} = \begin{cases} \min\left(\mathrm{h}_{E,K}^{\perp}, \mathrm{h}_{E,K'}^{\perp}\right), & \text{if} \quad E \in \mathcal{E}^{int}(\zeta), \quad E = \partial K \cap \partial K', \\ \mathrm{h}_{E,K}^{\perp}, & \text{if} \quad E \in \mathcal{E}(\zeta) \setminus \mathcal{E}^{int}(\zeta), \quad E = \partial K \cap \partial\Omega. \end{cases}$$

We then define $h_{\min,E}$ by

$$h_{\min,E} = \begin{cases} \min\left(h_{\min,K}, h_{\min,K'}\right), & \text{if} \quad E \in \mathcal{E}^{int}(\zeta), \quad E = \partial K \cap \partial K', \\ h_{\min,K}, & \text{if} \quad E \in \mathcal{E}(\zeta) \setminus \mathcal{E}^{int}(\zeta), \quad E = \partial K \cap \partial\Omega, \end{cases}$$

It is evident that the assumption (3) implies that for any edge $E \in \mathcal{E}(\zeta)$ and any element $K \in \zeta$, if $E \in \mathcal{E}(K)$ or E is a part of one element edge in K, one obtains

$$\mathrm{h}_E^{\perp} \sim \mathrm{h}_{E,K}^{\perp}, \qquad h_{\min,E} \sim h_{\min,K}. \tag{4}$$

2.2. Polynomial degrees

Now we introduce the polynomial degrees for the approximation in our DG method. Hence, for each element K of the mesh ζ we associate a polynomial degree $p_K \geq 1$ and we

introduce the degree vector $\mathbf{p} = \{ p_K : K \in \zeta \}$, with $|\mathbf{p}| = \max_{K\in\zeta} p_K$. We assume that $\mathbf{p}$ is of bounded local variation in the sense that for any pair of neighbouring elements $K, K' \in \zeta$, we have

$$\varrho^{-1} \leq \frac{p_K}{p_{K'}} \leq \varrho, \tag{5}$$

where $\varrho \geq 1$ is a constant independent of the particular mesh in a sequence of meshes. For any $E \in \mathcal{E}(\zeta)$, we introduce the edge polynomial degree p_E by

$$p_E = \begin{cases} \max\left(p_K, p_{K'}\right), & \text{if} \quad E = \partial K \cap \partial K' \in \mathcal{E}^{int}(\zeta), \\ \\ p_K, & \text{if} \quad E = \partial K \cap \partial\Omega \in \mathcal{E}(\zeta) \setminus \mathcal{E}^{int}(\zeta). \end{cases} \tag{6}$$

Hence, for a given partition ζ of Ω and a degree vector $\mathbf{p}$ on ζ, we define the *hp*-version DG finite element space by

$$V_{\mathbf{p}}(\zeta) = \Big\{ v \in L^2(\Omega) : \quad v|_K \in \mathcal{Q}_{p_K}(K), \quad K \in \zeta \Big\}, \tag{7}$$

with $\mathcal{Q}_{p_K}(K)$ denotes the set of all polynomials on the element K of degree less or equal to p_K in each direction.

2.3. Discrete problem

Next, we introduce the discrete version of problem (1). Let $\mathbf{n}_K$ denotes the outward unit normal on the boundary ∂K of an element K. Given an edge $E \in \mathcal{E}^{int}(\zeta)$ shared by two elements K^+ and K^-, a vector field $\mathbf{v} \in H^{1/2}(\Omega) \times H^{1/2}(\Omega)$ and a scalar field $v \in H^{1/2}(\Omega)$, we define the jumps and the averages of $\mathbf{v}$ and v across E by

$$\begin{aligned} \{v\} &= \frac{1}{2}\left(v\Big|_{\bar{K}^+} + v\Big|_{\bar{K}^-} \right), & [\![v]\!] &= v\Big|_{\bar{K}^+}\mathbf{n}_K + v\Big|_{\bar{K}^-}\mathbf{n}_{K'}, \\ \{A\mathbf{v}\} &= \left(\omega^- A\mathbf{v}\Big|_{\bar{K}^+} + \omega^+ A\mathbf{v}\Big|_{\bar{K}^-} \right), & [\![A\mathbf{v}]\!] &= A\mathbf{v}\Big|_{\bar{K}^+}\cdot\mathbf{n}_K + A\mathbf{v}\Big|_{\bar{K}^-}\cdot\mathbf{n}_{K'}, \end{aligned} \tag{8}$$

where $\omega^- = A^+/(A^+ + A^-)$ and $\omega^+ = A^-/(A^+ + A^-)$, with A^+, A^- are the values of A on the edge from either elements. Note that if $E \subset \partial\Omega$, we set $\{\mathbf{v}\} = \mathbf{v}$, $[\![\mathbf{v}]\!] = \mathbf{v}\cdot\mathbf{n}$, $\{v\} = v$ and $[\![v]\!] = v\mathbf{n}$, with $\mathbf{n}$ is the outward unit normal to the boundary $\partial\Omega$.

The derivation of the DG approximation for SP_1 and SP_3 equations can be performed using similar techniques as those reported in [9]. Thus, the DG approximation for the SP_1 problem reads as follows: Find $\phi_h \in V_{\mathbf{p}}(\zeta)$ such that

$$B\left(\phi_h, v_h\right) + K_h\left(\phi_h, v_h\right) = \left(F, v_h\right) + \sum_{E\in\mathcal{E}^{BC}(\zeta)} \int_E \frac{A}{C} G v_h \, ds, \qquad \forall v_h \in V_{\mathbf{p}}(\zeta) \ , \tag{9}$$

where the bilinear forms

$$B\left(w,v\right)=\sum_{K\in\zeta}\int_{K}\Big(A\nabla w\cdot\nabla v+Bwv\Big)\,d\mathbf{x}+\sum_{E\in\mathcal{E}^{int}(\zeta)}\frac{2\gamma\omega^{+}A^{+}p_{E}^{2}}{h_{E}^{\perp}}\int_{E}[\![w]\!]\cdot[\![v]\!]\,ds$$

$$+\sum_{E\in\mathcal{E}^{BC}(\zeta)}\int_{E}\frac{AD}{C}wv\,ds, \tag{10}$$

$$K_{h}\left(w,v\right)=-\sum_{E\in\mathcal{E}^{int}(\zeta)}\int_{E}\{A\nabla w\}\cdot[\![v]\!]+\{A\nabla v\}\cdot[\![w]\!]\,ds,$$

and where $(\cdot,\cdot)$ denotes the standard linear form and where γ is the penalty term constant. In order to obtain a stable DG method for meshes with anisotropic elements, the penalty term $\frac{2\gamma\omega^{+}A^{+}p_{E}^{2}}{h_{E}^{\perp}}\int_{E}[\![w]\!]\cdot[\![v]\!]\,ds$ involves $h_{E}^{\perp}$, the measure of the elements perpendicularly to the edge E, rather than the size of the edge itself. For isotropic shape regular meshes, the two choices are equivalent, but for anisotropic meshes it is no longer the case. Similarly, the DG approximation for the SP_3 system reads as follows: Find $\phi_h\in V_{\mathbf{p}}(\zeta)\times V_{\mathbf{p}}(\zeta)$ such that

$$B\left(\phi_h,v_h\right)+K_{h}\left(\phi_h,v_h\right)=\left(F,v_h\right)+\sum_{E\in\mathcal{E}^{BC}(\zeta)}\int_{E}\frac{A}{C}Gv_h\,ds,\qquad\forall v_h\in V_{\mathbf{p}}(\zeta)\times V_{\mathbf{p}}(\zeta), \tag{11}$$

where the bilinear form are the vectorial version of (10). Considering the DG norm:

$$\begin{aligned}|||u|||_{\zeta}=\Bigg(&\sum_{K\in\zeta}\left(\left\|A^{1/2}\nabla u\right\|_{0,K}^{2}+\left\|B^{1/2}u\right\|_{0,K}^{2}\right)\\&+\sum_{E\in\mathcal{E}^{int}(\zeta)}\left\|\Big(\frac{\gamma2\omega^{+}A^{+}p_{E}^{2}}{h_{E}^{\perp}}\Big)^{1/2}[\![u]\!]\right\|_{0,E}^{2}+\sum_{E\in\mathcal{E}^{BC}(\zeta)}\left\|\Big(\frac{AD}{C}\Big)^{1/2}u\right\|_{0,E}^{2}\Bigg)^{1/2},\end{aligned} \tag{12}$$

where $\|\cdot\|_{0,K}$ and $\|\cdot\|_{0,E}$ are respectively the L^2-norm on an element K and on an edge E. It is possible to prove coercivity for the lhs of problem (9) for $\gamma>0$ large enough reworking Theorem 3.5 in [22]. Moreover, it is also possible to prove continuity for the lhs of problem (9) applying the Cauchy-Schwarz inequality. The results can be easily extended to the SP_3 when the DG norm (12) is applied.

3. Anisotropic a-posteriori error estimate

The error estimator presented in this section is designed to work on meshes with anisotropic elements, this is particularly useful in view of the fact that steep radiative gradients and boundary layers are very common in the SP_1 and the SP_3 approximations of radiative transfer. Without the freedom to use anisotropic elements, the numerical method would needed extremely refined meshes to resolve these features. Moreover, in order to improve the convergence speed, both the DG method and the error estimator allow for elements with different orders of polynomials in the same meshes.

Remark 3.1. *From now on the notation $a \lesssim b$ is used to denote $a \leq c\,b$, where c is a constant that may depend on the coefficients in (1), the value of γ and the constants in the coercivity and the continuity results of the lhs of problems (9) and (11). The constant c is always independent of the sizes of the elements and the orders of polynomials in the elements.*

The error estimator for the SP_1 and the SP_3 problems is given by

$$\eta_{\text{err}} = \sqrt{\sum_{K\in\zeta} \left(\eta_{R,K}^2 + \eta_{B,K}^2 + \eta_{E,K}^2 + \eta_{J,K}^2\right)}, \tag{13}$$

where the four terms under the sum are defined as

$$\begin{aligned}
\eta_{R,K}^2 &= \alpha_K^2 \left\| F_h + \nabla\cdot(A\nabla\phi_h) - B\phi_h \right\|_{0,K}^2,\\
\eta_{B,K}^2 &= \sum_{E\in\mathcal{E}^{BC}(K)} A_{\min}^{-1/2}\alpha_E \left\| A\nabla\phi_h\cdot\mathbf{n}_E + \frac{AD}{C}\phi_h - \frac{A}{C}G_h \right\|_{0,E}^2 + \sum_{E\in\mathcal{E}^{\mathrm{BC}}(K)} \left\| \left(\frac{AD}{C}\right)^{1/2}\phi_h - I_{hp}\phi_h \right\|_{0,E}^2\\
&\quad + \sum_{E\in\mathcal{E}^{\mathrm{BC}}(K)} \left(\frac{A_{\max}h_{E,K}^{\perp}p_E^2}{h_{\min,\mathrm{K}}^2} + \frac{\kappa_{\max}h_{E,K}^{\perp}}{p_E^2} \right) \left\| \phi_h - I_{hp}\phi_h \right\|_{0,E}^2\\
\eta_{E,K}^2 &= \sum_{E\in\mathcal{E}^{\mathrm{int}}(K)} A_{\min}^{-1/2}\alpha_E \left\| [\![A\nabla\phi_h]\!] \right\|_{0,E}^2,\\
\eta_{J,K}^2 &= \frac{1}{2}\sum_{E\in\mathcal{E}^{\mathrm{int}}(K)} \left(\frac{\gamma^2 A_{\max}p_E^2}{h_{E,K}^{\perp}} + \frac{A_{\max}h_{E,K}^{\perp}p_E^2}{h_{\min,\mathrm{K}}^2} + \frac{\kappa_{\max}h_{E,K}^{\perp}}{p_E^2} + \frac{A_{\max}p_E^2}{h_{E,K}^{\perp}} + \frac{A_{\max}\gamma^2 p_E^3}{h_{E,K}^{\perp}} \right) \left\| [\![\phi_h]\!] \right\|_{0,E}^2,
\end{aligned}$$

with A, B, C, D, F, G and ϕ defined either for the SP_1 or the SP_3, with F_h and G_h the L^2 projection of F and G onto the finite element space and with $I_{hp}\phi_h$ the continuous interpolation of ϕ_h defined in (15) and (16). Here, $A_{\min}$ and $A_{\max}$ are the minimum and the maximum eigenvalues of all the values of the matrix A on the elements containing an edge and

$$\alpha_K = \min\left(h_{\min,K}A_{\min}^{-\frac{1}{2}}p_K^{-1}, {\kappa_{\min}}^{-\frac{1}{2}}\right), \qquad \alpha_E = \min\left(h_{\min,K}^2 {A_{\min}}^{-\frac{1}{2}} p_E^{-1}\left(h_E^{\perp}\right)^{-1}, {\kappa_{\min}}^{-\frac{1}{2}}\right),$$

where $\kappa_{\min}$ and $\kappa_{\max}$ are the minimum and the maximum values of κ on the computational domain Ω.

Next, we introduce the reliability result, which is the main result of the paper.

Theorem 3.2. *Let ϕ the exact solution and ϕ_h the computed solution for either the SP_1 or the SP_3 problem, we have that*

$$|||\phi - \phi_h|||_{\zeta} \leq C\left(\eta_{\text{err}} + \Theta\right),$$

where C is a positive constant independent of the mesh nor the order of the elements used and

$$\Theta = \sqrt{\sum_{K\in\zeta}\Theta_K^2 + \sum_{E\in\mathcal{E}^{BC}(\zeta)}\Theta_B^2},$$

where

$$\Theta_K^2 = \alpha_K^2 \Big\| F - F_h \Big\|_{0,K}^2, \quad \Theta_B^2 = \frac{h_{\min,K}^2}{A_{\min} p_E^2 h_{E,K}^{\perp}} \Big\| G - G_h \Big\|_{0,E}^2,$$

is the data oscillations term.

The rest of the section is devoted to the proof of Theorem 3.2. Similarly to the approach in [23, 24, 8], the first step is to introduce an auxiliary irregular mesh $\widetilde{\zeta}$. Such mesh is obtained from ζ as follows. For any $K \in \zeta$ if all four elemental edges are edges of the mesh ζ, then we include K untouched into $\widetilde{\zeta}$. Otherwise, at least one of the elemental edges of K contains a hanging node. In this case, we replace K by the four quadrilateral elements obtained from bisecting the elemental edges of K. By construction, the mesh $\widetilde{\zeta}$ is a refinement of ζ. Moreover, the hanging nodes of ζ are not hanging nodes of $\widetilde{\zeta}$ any more. Then, we define DG finite element space on the mesh $\widetilde{\zeta}$:

$$V_{\mathbf{p}}(\widetilde{\zeta}) = \Big\{ v \in L^2(\Omega) : \quad v|_{\widetilde{K}} \in \mathcal{Q}_{\widetilde{p}_{\widetilde{K}}}(\widetilde{K}), \quad \widetilde{K} \in \widetilde{\zeta} \Big\},$$

where the auxiliary polynomial degree $\widetilde{p}_{\widetilde{K}}$ is defined by $\widetilde{p}_{\widetilde{K}} = p_K$ for K the element in ζ containing $\widetilde{K}$. We clearly have the following inclusion:

$$V_{\mathbf{p}}(\zeta) \subseteq V_{\mathbf{p}}(\widetilde{\zeta}). \tag{14}$$

From the definition of the auxiliary mesh $\widetilde{\zeta}$ and on the auxiliary space $V_{\mathbf{p}}(\widetilde{\zeta})$, the following result, which is derived from [24, Lemma 4.2, Lemma 4.3], is straightforward.

Lemma 3.3. *For the* SP_1 *case, let* $v \in V_{\mathbf{p}}(\widetilde{\zeta}) + H^1(\Omega)$ *be such that* $[\![v]\!]|_E = [\![w]\!]|_E$ *for all* $E \in \mathcal{E}(\widetilde{\zeta})$*, for a function* $w \in V_{\mathbf{p}}(\zeta) + H^1(\Omega)$*. Then we have*

$$\sum_{E \in \mathcal{E}^{int}(\zeta)} \frac{2\gamma\omega^+ A^+ p_E^2}{h_E^{\perp}} \int_E [\![w]\!]^2 \, ds \lesssim \sum_{\widetilde{E} \in \mathcal{E}^{int}(\widetilde{\zeta})} \frac{2\gamma\omega^+ A^+ p_{\widetilde{E}}^2}{h_{\widetilde{E}}^{\perp}} \int_{\widetilde{E}} [\![v]\!]^2 \, ds \lesssim \sum_{E \in \mathcal{E}^{int}(\zeta)} \frac{2\gamma\omega^+ A^+ p_E^2}{h_E^{\perp}} \int_E [\![w]\!]^2 \, ds \, .$$

There is an analogue result for the SP_3 *case with* $v \in [V_{\mathbf{p}}(\widetilde{\zeta}) + H^1(\Omega)]^2$ *and* $w \in [V_{\mathbf{p}}(\zeta) + H^1(\Omega)]^2$ *where the inequalities hold for all components.*

A straightforward consequence of Lemma 3.3 is the next lemma.

Lemma 3.4. *For* $v \in V_{\mathbf{p}}(\zeta) + H^1(\Omega)$*, we have the bounds*

$$|||v|||_{\zeta} \lesssim |||v|||_{\widetilde{\zeta}}.$$

A fundamental ingredient for the proof of Theorem 3.2 is the choice of the right averaging operator. In the present work we use a variation of the averaging operator for anisotropic meshes presented in [8]. The extension is necessary since such operator projects functions from the DG finite element space onto $V_{\mathbf{p}}(\widetilde{\zeta}) \cap H_0^1(\Omega)$. For the problem considered in this paper, this is not suitable because the boundary conditions of (1) are not homogeneous

Dirichlet. We need an averaging operator $I_{hp} : V_{\mathbf{p}}(\zeta) \to V^c_{\mathbf{p}}(\widetilde{\zeta}) \equiv V_{\mathbf{p}}(\widetilde{\zeta}) \cap H^1(\Omega)$. In order to achieve our goal, we need to modify the way in which $I_{hp}v$, with $v \in V_{\mathbf{p}}(\zeta)$, is constructed in [8]. The construction of the function $I_{hp}v$ in [8] is done summing three parts: $I_{hp}v = \nu^{\text{nodes}} + \nu^{\text{edges}} + \nu^{\text{int}}$, where respectively ν^{nodes} is the approximation of v on the nodes of the mesh, ν^{edges} on the edges and ν^{int} in the interior of the elements. The details can be found in [25, Section 5.5]. The component ν^{int} coincides with v in the interior of the elements, since also v is conforming in the interior of the elements. But to ensure global conformity, ν^{nodes} and ν^{edges} are the averages of the values of v on the nodes and on the edges. The analysis in [25, Section 5.5] for ν^{nodes} and ν^{edges} on edges in the interior of the domain can be applied also in our case. Unfortunately this is not true on the boundary of the domain where a different type of boundary condition is applied. By construction in [8] the value of $I_{hp}v$ along the boundary $\partial\Omega$ is zero, instead for the choice of spaces used here we have in general that $I_{hp}v$ is not zero along the boundary, but rather a conforming projection of the value of v. In this new setting, applying the argument in [25, Section 5.5], we obtain the following inequalities:

$$\sum_{\widetilde{K}\in\widetilde{\zeta}} \|v - I_{hp}v\|^2_{L^2(\widetilde{K})} \lesssim \sum_{E\in\mathcal{E}^{\text{int}}(\zeta)} \int_E p_E^{-2} h_E^{\perp} [\![v]\!]^2 \, ds + \sum_{E\in\mathcal{E}^{\text{BC}}(\zeta)} \int_E p_E^{-2} h_E^{\perp} (v - I_{hp}v)^2 \, ds, \quad (15)$$

$$\sum_{\widetilde{K}\in\widetilde{\zeta}} \|\nabla(v - I_{hp}v)\|^2_{L^2(\widetilde{K})} \lesssim \sum_{E\in\mathcal{E}^{\text{int}}(\zeta)} \int_E p_E^{2} h_E^{\perp} h_{\min,E}^{-2} [\![v]\!]^2 \, ds + \sum_{E\in\mathcal{E}^{\text{BC}}(\zeta)} \int_E p_E^{2} h_E^{\perp} h_{\min,E}^{-2} (v - I_{hp}v)^2 \, ds. \quad (16)$$

Comparing (15) and (16) with the corresponding results in [8], we have that the terms on edges on the boundary are different, this is precisely because $I_{hp}v$ is not zero along the boundary.

Following [26, 27], we decompose the discontinuous Galerkin solution into a conforming part and a remainder:

$$\phi_h = \phi_h^c + \phi_h^r, \quad (17)$$

where $\phi_h^c = I_{hp}\phi_h \in V^c_{\mathbf{p}}(\widetilde{\zeta}) \subset H^1(\Omega)$. The remainder is then given by $\phi_h^r = \phi_h - \phi_h^c = \phi_h - I_{hp}\phi_h \in V_{\mathbf{p}}(\widetilde{\zeta})$. By Lemma 3.4 and the triangle inequality, we obtain

$$|||\phi - \phi_h|||_{\zeta} \lesssim |||\phi - \phi_h|||_{\widetilde{\zeta}} \lesssim |||\phi - \phi_h^c|||_{\widetilde{\zeta}} + |||\phi_h^r|||_{\widetilde{\zeta}} = |||\phi - \phi_h^c|||_{\zeta} + |||\phi_h^r|||_{\widetilde{\zeta}}. \quad (18)$$

The next series of lemmas contains the profs that both the conforming error $\phi - \phi_h^c$ and the remainder ϕ_h^r can be bounded by the estimator η_{err}.

Lemma 3.5. *For both the* SP_1 *case and the* SP_3 *case it is possible to prove:*

$$||\phi_h^r|||_{\widetilde{\zeta}} \lesssim \eta_{\text{err}}.$$

Proof. Only the proof for the SP_1 case is presented here, the proof for the SP_3 case follows similarly. Since $[\![\phi_h^r]\!]|_E = [\![\phi_h]\!]|_E$ for all $E \in \mathcal{E}(\widetilde{\zeta})$ and $\phi_h \in V_{\mathbf{p}}(\zeta)$, yield

$$\sum_{\widetilde{E}\in\mathcal{E}^{\text{int}}(\widetilde{\zeta})} \left\| \left(\frac{\gamma 2\omega^+ A^+ p_{\widetilde{E}}^2}{h_{\widetilde{E}}^{\perp}} \right)^{1/2} [\![\phi_h^r]\!] \right\|^2_{0,\widetilde{E}} \lesssim \gamma^{-1} \sum_{E\in\mathcal{E}^{\text{int}}(\zeta)} \left\| \left(\frac{\gamma^2 2\omega^+ A^+ p_E^2}{h_E^{\perp}} \right)^{1/2} [\![\phi_h]\!] \right\|^2_{0,E}.$$

From (15) and (16), we have

$$\sum_{\widetilde{K}\in\widetilde{\zeta}} \|A^{1/2}\nabla\phi_h^r\|_{0,\widetilde{K}}^2 \lesssim \sum_{E\in\mathcal{E}^{\rm int}(\zeta)} \frac{p_E^2 h_E^\perp A_{\max}}{h_{\min,E}^2}\|[\![\phi_h]\!]\|_{0,E}^2 + \sum_{E\in\mathcal{E}^{\rm BC}(\zeta)} \frac{p_E^2 h_E^\perp A_{\max}}{h_{\min,E}^2}\|\phi_h - I_{hp}\phi_h\|_{0,E}^2,$$

$$\sum_{\widetilde{K}\in\widetilde{\zeta}} \|B^{1/2}\phi_h^r\|_{0,\widetilde{K}}^2 \lesssim \sum_{E\in\mathcal{E}^{\rm int}(\zeta)} \frac{h_E^\perp \kappa_{\max}}{p_E^2}\|[\![\phi_h]\!]\|_{0,E}^2 + \sum_{E\in\mathcal{E}^{\rm BC}(\zeta)} \frac{h_E^\perp \kappa_{\max}}{p_E^2}\|\phi_h - I_{hp}\phi_h\|_{0,E}^2.$$

Hence, the statement of the lemma follows from the definitions of the jump residual $\eta_{J,K}$ and the jump boundary $\eta_{B,K}$.

□

To prove Theorem 3.2, we also need the following inequalities proven in Lemma 8 in [8].

Lemma 3.6 (Local interpolation error bounds)**.** *For any function $v \in H^1(\Omega)$, there exists a function $v_{hp} \in V_{\mathbf{p}}(\zeta)$ such that*

$$\begin{aligned} p_K^2\|v - v_{hp}\|_{0,K}^2 &\lesssim \|\mathbf{M}_K\nabla v\|_{0,K}^2, \\ \|\mathbf{M}_K\nabla(v - v_{hp})\|_{0,K}^2 &\lesssim \|\mathbf{M}_K\nabla v\|_{0,K}^2, \\ \sum_{E\in\mathcal{E}(K)} h_{E,K}^\perp p_E\|v - v_{hp}\|_{0,E}^2 &\lesssim \|\mathbf{M}_K\nabla v\|_{0,K}^2, \end{aligned} \tag{19}$$

for any $K \in \zeta$.

Let's introduced the alignment measure already defined in [8]:

$$\mathcal{M}(v,\zeta) = \frac{\left(\sum_{K\in\zeta} h_{\min,K}^{-2}\|\mathbf{M}_K\nabla v\|_{0,K}^2\right)^{1/2}}{\|\nabla v\|_{0,\Omega}}.$$

It is clear from the definition that

$$1 \le \mathcal{M}(v,\zeta) \lesssim \max_{K\in\zeta}\frac{h_{\max,K}}{h_{\min,K}} \quad \forall v \in H^1(\Omega).$$

Then the global interpolation error estimation follows from Lemma 3.6 and the definition of the alignment measure.

Lemma 3.7 (Global interpolation error bounds)**.** *For any function $v \in H^1(\Omega)$, we have*

$$\begin{aligned} \sum_{K\in\zeta}\frac{p_K^2}{h_{\min,K}^2}\|v - v_{hp}\|_{0,K}^2 &\lesssim \mathcal{M}(v,\zeta)^2\|\nabla v\|_{0,\Omega}^2, \\ \sum_{K\in\zeta}\sum_{E\in\partial K}\frac{h_{E,K}^\perp p_E}{h_{\min,K}^2}\|v - v_{hp}\|_{0,E}^2 &\lesssim \mathcal{M}(v,\zeta)^2\|\nabla v\|_{0,\Omega}^2. \end{aligned} \tag{20}$$

We then have the following result.

Lemma 3.8. *For the* SP_1 *case we have that for any* $v \in H^1(\Omega)$*, we have*

$$\int_\Omega F(v-v_h)\,d\mathbf{x}+\int_{\partial\Omega}\frac{A}{C}G(v-v_h)ds-B(\phi_h,v-v_h)+K_h(\phi_h,v_h)\lesssim \mathcal{M}(v,\zeta)\,(\eta_{\mathrm{err}}+\Theta)\,|||v|||_\zeta.$$

Here, $v_h \in V_{\mathbf{p}}(\zeta)$ *is the hp-interpolant of* v *in Lemma 3.6. A similar result hold also for the* SP_3 *case.*

Proof. Integration by parts of the diffusive volume terms readily yields

$$\int_\Omega F(v-v_h)\,d\mathbf{x}+\int_{\partial\Omega}\frac{A}{C}G(v-v_h)ds-B(\phi_h,v-v_h)+K_h(\phi_h,v_h)=T_1+T_2+T_3+T_4+T_5,$$

where

$$T_1=\sum_{K\in\zeta}\int_K (F+\nabla\cdot(A\nabla\phi_h)-B\phi_h)(v-v_h)\,d\mathbf{x},$$

$$T_2=-\sum_{E\in\mathcal{E}^{\mathrm{int}}(\zeta)}\int_E [\![A\nabla\phi_h]\!]\{\!\{v-v_h\}\!\}\,ds,$$

$$T_3=-\sum_{E\in\mathcal{E}^{\mathrm{int}}(\zeta)}\int_E \{\!\{A\nabla v_h\}\!\}\cdot[\![\phi_h]\!]\,ds,$$

$$T_4=-\sum_{E\in\mathcal{E}^{\mathrm{BC}}(\zeta)}\int_E A\nabla\phi_h\cdot\mathbf{n}_E(v-v_h)\,ds-\int_{\partial\Omega}\frac{AD}{C}\phi_h(v-v_h)\,ds+\int_{\partial\Omega}\frac{A}{C}G(v-v_h)\,ds,$$

$$T_5=-\sum_{E\in\mathcal{E}^{\mathrm{int}}(\zeta)}\int_E \frac{\gamma 2\omega^+A^+p_E^2}{h_E^\perp}[\![\phi_h]\!]\cdot[\![v-v_h]\!]\,ds.$$

To bound T_1 can be achieved in two ways, the way resulting in the sharper bound is used. Following the first way we first add and subtract the data approximations and then we apply the weighted Cauchy-Schwarz inequality and the approximation properties in (20) to obtain

$$T_1\lesssim \mathcal{M}(v,\zeta)\Big(\sum_{K\in\zeta}(\eta_{R,K}^2+\Theta_K^2)\Big)^{\frac{1}{2}}|||v|||_\zeta. \tag{21}$$

The details are not included here because it is the same argument used to bound the term T_1 in [27, Lemma 4.8]. The second way exploits the fact that $\|v-v_h\|_{0,K}\le\|v\|_{0,K}$, then we have

$$T_1\le\sum_{K\in\zeta}\kappa_{\min}^{-1/2}\|F+\nabla\cdot(A\nabla\phi_h)-B\phi_h\|_{0,K}\kappa_{\min}^{1/2}\|v\|_{0,K}\le\sum_{K\in\zeta}\kappa_{\min}^{-1/2}\|F+\nabla\cdot(A\nabla\phi_h)-B\phi_h\|_{0,K}|||v|||_\zeta.$$

From here the same bound (21) can be found using the fact $1\le\mathcal{M}(v,\zeta)$. As for the term T_1, there are two ways to bound the term T_2 as well. The first way leads to

$$T_2\lesssim \mathcal{M}(v,\zeta)\Big(\sum_{K\in\zeta}\eta_{E,K}^2\Big)^{\frac{1}{2}}|||v|||_\zeta, \tag{22}$$

and it is presented in [8, Lemma 14]. The second way exploits the fact that $1 \leq p_E h_{E,K}^{\perp} h_{\min,K}^{-2}$:

$$T_2 \lesssim \sum_{E \in \mathcal{E}^{\mathrm{int}}(\zeta)} A_{\min}^{-1/2} \kappa_{\min}^{-1/2} \|[\![A\nabla\phi_h]\!]\|_{0,E} \kappa_{\min}^{1/2} \Big(\frac{A p_E h_{E,K}^{\perp}}{h_{\min,K}^2}\Big)^{1/2} \|v - v_h\|_{0,E},$$

then the bound (22) is also achieved using (20). The term T_3 is bounded as in [8, Lemma 14]:

$$T_3 \lesssim \Big(\sum_{K \in \zeta} \eta_{J,K}^2\Big)^{\frac{1}{2}} |||v|||_{\zeta}.$$

Also for T_4 there are two ways to bound it. In the first way we first add and subtract the data approximations and then we apply the weighted Cauchy-Schwarz inequality:

$$\begin{aligned}
|T_4| = \Bigg| &- \sum_{E \in \mathcal{E}^{\mathrm{BC}}(\zeta)} \int_E A\nabla\phi_h \cdot \mathbf{n}_E (v - v_h)\, ds - \int_{\partial\Omega} \frac{AD}{C} \phi_h (v - v_h)\, ds + \int_{\partial\Omega} \frac{A}{C} G_h (v - v_h)\, ds \Bigg| \\
&+ \sum_{E \in \mathcal{E}^{\mathrm{BC}}(\zeta)} \int_E \frac{A}{C} (G - G_h)(v - v_h)\, ds \\
\lesssim &\Bigg(\sum_{E \in \mathcal{E}^{\mathrm{BC}}(\zeta)} \Bigg(\frac{h_{\min,K}^2}{A_{\min} p_E h_{E,K}^{\perp}} \| - A\nabla\phi_h \cdot \mathbf{n}_E - \frac{AD}{C}\phi_h + \frac{A}{C} G_h \|_{0,E}^2 \Bigg)^{1/2} \\
&+ \sum_{E \in \mathcal{E}^{\mathrm{BC}}(\zeta)} \Bigg(\frac{h_{\min,K}^2}{A_{\min} p_E h_{E,K}^{\perp}} \|G - G_h\|_{0,E}^2 \Bigg)^{1/2} \Bigg(\frac{A_{\min} p_E h_{E,K}^{\perp}}{h_{\min,K}^2} \|v - v_h\|_{0,E}^2 \Bigg)^{1/2}.
\end{aligned}$$

The using (20) we get:

$$T_4 \lesssim \mathcal{M}(v,\zeta) \Big(\sum_{K \in \zeta} (\eta_{B,K}^2 + \Theta_B^2) \Big)^{\frac{1}{2}} |||v|||_{\zeta}. \tag{23}$$

The second way to get (23) is analogues to the second way to bound T_2.

Finally, we have the bound for T_5 which is reached as in [8, Lemma 14].

$$T_5 \lesssim \mathcal{M}(v,\mathcal{T}) \Big(\sum_{K \in \mathcal{T}} \eta_{J_K}^2 \Big)^{\frac{1}{2}} |||v|||_{\zeta}.$$

The above estimations for the terms T_1 through T_5 imply the assertion. □

The last result needed to prove Theorem 3.2 is the following lemma.

Lemma 3.9. *For both the the* SP_1 *case and the* SP_3 *case hold:*

$$|||\phi - \phi_h^c|||_{\zeta} \lesssim \mathcal{M}(v,\zeta)(\eta_{\mathrm{err}} + \Theta).$$

Proof. As done so far, only the SP_1 is considered in the proof, the SP_3 follows similarly. Since $\phi - \phi_h^c \in H^1(\Omega)$ we have that:

$$|||\phi - \phi_h^c|||_\zeta^2 = \int_\Omega A(\nabla(\phi - \phi_h^c))^2 + B(\phi - \phi_h^c)^2 \, d\mathbf{x} + \int_{\partial\Omega} \frac{AD}{C}(\phi - \phi_h^c)^2 \, ds.$$

Now, considering the weak form of the continuous problem (1), i.e.:

$$\int_\Omega A\nabla\phi \cdot \nabla v + B\phi v \, d\mathbf{x} + \int_{\partial\Omega} \frac{AD}{C}\phi v \, ds = \int_\Omega Fv \, d\mathbf{x} + \int_{\partial\Omega} \frac{A}{C} Gv \, ds \ ,$$

we have

$$|||\phi - \phi_h^c|||_\zeta |||v|||_\zeta = \int_\Omega Fv \, d\mathbf{x} + \int_{\partial\Omega} \frac{A}{C} Gv \, ds - \int_\Omega A\nabla\phi_h^c \cdot \nabla v + B\phi_h^c v \, d\mathbf{x} - \int_{\partial\Omega} \frac{AD}{C}\phi_h^c v \, ds,$$

where $v = \phi - \phi_h^c$. In view of (9) and the fact that $\phi_h^c \in H^1(\Omega)$, this is equivalent to

$$|||\phi - \phi_h^c|||_\zeta |||v|||_\zeta = \int_\Omega Fv \, d\mathbf{x} + \int_{\partial\Omega} \frac{A}{C} Gv \, ds - B(\phi_h^c, v),$$

where

$$B(\phi_h^c, v) = B(\phi_h, v) + R,$$

with

$$R = -\sum_{\tilde{K}\in\tilde{\zeta}} \int_{\tilde{K}} \left(A\nabla\phi_h^r \cdot \nabla v + B\phi_h^r v \right) d\mathbf{x} - \int_{\partial\Omega} \frac{AD}{C}\phi_h^r v \, ds.$$

Subtracting (9), yields:

$$|||\phi - \phi_h^c|||_\zeta |||v|||_\zeta = \int_\Omega F(v - v_h) \, d\mathbf{x} + \int_{\partial\Omega} \frac{A}{C} G(v - v_h) \, ds - B(\phi_h, v - v_h) + K_h(\phi_h, v_h) - R, \quad (24)$$

with v_h the DG approximation of v. The term R can be bounded using Cauchy-Schwarz and Lemma 3.5 as

$$|R| \lesssim |||\phi_h^r|||_\zeta |||v|||_\zeta \lesssim \eta_{\mathrm{err}} |||v|||_\zeta \ . \quad (25)$$

The proof is concluded applying Lemma 3.8 and (25) to (24). □

Finally, the proof of Theorem 3.2 now immediately follows from the inequality (18), Lemma 3.5 and Lemma 3.9.

4. Numerical experiments

In this section we analyse the *hp*-adaptive numerical method described in the previous sections. To simplify the implementation , we are going to use the following error estimator, which is a modification of the error estimator η_{err} defined in (13):

$$\tilde{\eta}_{\mathrm{err}} = \sqrt{\sum_{K\in\zeta} \left(\eta_{R,K}^2 + \tilde{\eta}_{B,K}^2 + \eta_{E,K}^2 + \eta_{J,K}^2 \right)}, \quad (26)$$

the difference consists in the term $\tilde{\eta}_{B,K}$ that is defined as

$$\tilde{\eta}^2_{B,K} = \sum_{E\in\mathcal{E}^{BC}(K)} A_{\min}^{-1/2}\alpha_E \left\| A\nabla\phi_h\cdot\mathbf{n}_E + \frac{AD}{C}\phi_h - \frac{A}{C}G_h \right\|^2_{0,E},$$

which is the term $\eta_{B,K}$ with the two terms containing $I_{hp}\phi_h$ removed. The quantity $I_{hp}\phi_h$ is expensive to compute and for this reason it has been removed. However, as can be seen from the results in the rest of the section, and especially from the efficiency plots, the omission of such terms do not ruin the performances of the method.

The implementation of the method has been done in the `AptoFEM` software package. The resulting discrete systems of linear equations are solved by exploiting the Multifrontal Massively Parallel Solver (MUMPS), see for example [28, 29, 30]. We consider different adaptive techniques for the SP_1 and SP_3 approximations, namely: isotropic h-adaptivity, isotropic hp-adaptivity, anisotropic h-adaptivity, anisotropic h isotropic p-adaptivity and uniform h-adaptivity. In all our computations the meshes are adapted by marking the elements for refinement according to the size of the local error indicators. This is achieved by employing the fixed fraction strategy proposed in [31], with a refinement fraction of 15%. Thus, for each element $K \in \zeta$ marked for refinement the schemes automatically decide whether the local mesh size h_K or the local polynomial degree p_K should be adjusted accordingly. The choice to perform either h- or p-refinement is based on estimating the local smoothness of the (unknown) analytical solution. To this end, we employ the hp-adaptive strategy developed in [32], where the local regularity of the analytical solution is estimated from truncated local Legendre expansions of the computed numerical solution. This is accomplished computing the decay rate of the coefficients of the local Legendre expansions, then if the speed is faster than a threshold σ the solution is considered locally smooth and p-refinement is applied, otherwise, the solution is not considered locally smooth enough and h-refinement is applied. Furthermore, if anisotropic h-refinement is considered in the scheme, there is a further choice to make for each element qualified for refinement in h between isotropic h-refinement or anisotropic h-refinement. In order to make this choice we denote by $\mathcal{E}^1_K$, $\mathcal{E}^2_K$ the two sets containing opposite edges of the element K, and we define

$$\eta_{\mathcal{E}^i_K} = \sqrt{\eta^2_{E,K}\Big|_{\mathcal{E}^i_K} + \tilde{\eta}^2_{B,K}\Big|_{\mathcal{E}^i_K} + \eta^2_{J,K}\Big|_{\mathcal{E}^i_K}}, \qquad i = 1, 2.$$

Then the choice between isotropic h-refinement or anisotropic h-refinement is made comparing the error quantities $\eta_{\mathcal{E}^i_K}$ $(i = 1, 2)$ as:

(i) If $\eta_{\mathcal{E}^1_K} > 100\eta_{\mathcal{E}^2_K}$, then the element K is refined anisotropically along the direction $\underline{v}^1_K$.

(ii) If $\eta_{\mathcal{E}^2_K} > 100\eta_{\mathcal{E}^1_K}$, then the element K is refined anisotropically along the direction $\underline{v}^2_K$.

(iii) If none of the above conditions (i) and (ii) is satisfied, the element K is refined isotropically.

In all examples, the emphasis will be on investigating the asymptotic efficiency of the proposed a-posteriori error estimator. To this end, we compute the efficiency index, i.e. $\tilde{\eta}_{\text{err}}/|||\phi - \phi_h|||_\zeta$, which should be bounded with not too big oscillations on the sequence of adaptively refined meshes as a consequence of Theorem 3.2 that links the value true error to the value of the error estimator.

4.1. Example 1

The first problem can be considered simple because it does not have any anisotropic feature. We first solve the SP_1 problem in an unit squared domain using $\sigma = \kappa = 1$, $\varepsilon = 1$ and $r_1 = r_2 = 0$. The functions F and G in the right-hand side of equations (1) are calculated such that the analytical solution of the SP_1 problem is given by

$$\varphi(x, y) = \cos(2\pi x)\cos(2\pi y).$$

In Figure 2a we present the convergence of the errors using different refinement techniques. We consider isotropic h-adaptivity and isotropic hp-adaptivity with two choices for the parameter σ from [32]. The value of σ determines the balance between h and p adaptivity and this has an impact on the overall convergence rate. Higher values of σ correspond to more p-refinement and for smooth problems like the one considered here a faster convergence. Since the solution does not have any anisotropic behaviour, the only adaptive techniques tested in this case are isotropic hp-adaptivity and isotropic h-adaptivity. It is clear that there is a huge difference between these adaptive techniques, the former converges exponentially whereas the other only polynomially. In Figure 2b there is the efficiency plot for isotropic hp-adaptivity, it is clear that the efficiency index is well bounded, as expected from the theory.

In Figure 3 we present the solution for SP_1, the final isotropically hp-adapted mesh and the final isotropiccally h-adapted mesh. In both cases the refined patterns follows closely the features of the solution.

The second problem is an extension of the first one to the SP_3 case. Hence, we solve equations (1) on a unit square using $\varepsilon = 1$, $\sigma = \kappa = 1$, $\alpha_1 = \alpha_2 = \beta_1 = \beta_2 = 1$ and $\mu_1 = \mu_2 = 1$. The right-hand side F and boundary function G in (1) are analytically evaluated such that the exact solution of the SP_3 equations is

$$\begin{aligned} \psi_1(x, y) &= \cos(2\pi x)\cos(2\pi y), \\ \psi_2(x, y) &= \cos(2\pi x)\cos(2\pi y). \end{aligned}$$

In Figure 4a we present the convergence of the errors using different refinement techniques. Since also in this case the solution does not have any anisotropic behaviour, the only adaptive techniques tested in this case are isotropic hp-adaptivity for values of $\sigma = 0.8, 1$ and isotropic h-adaptivity. It is clear, as in the previous case, that there is a huge difference between these adaptive techniques and that the isotropic hp-adaptive one converges much faster. In Figure 4b there is also the efficiency plot for isotropic hp-adaptivity.

In Figure 5 we present the final isotropically hp-adapted mesh and the final isotropically h-adapted mesh. Also here, the refined patterns follows closely the features of the solution.

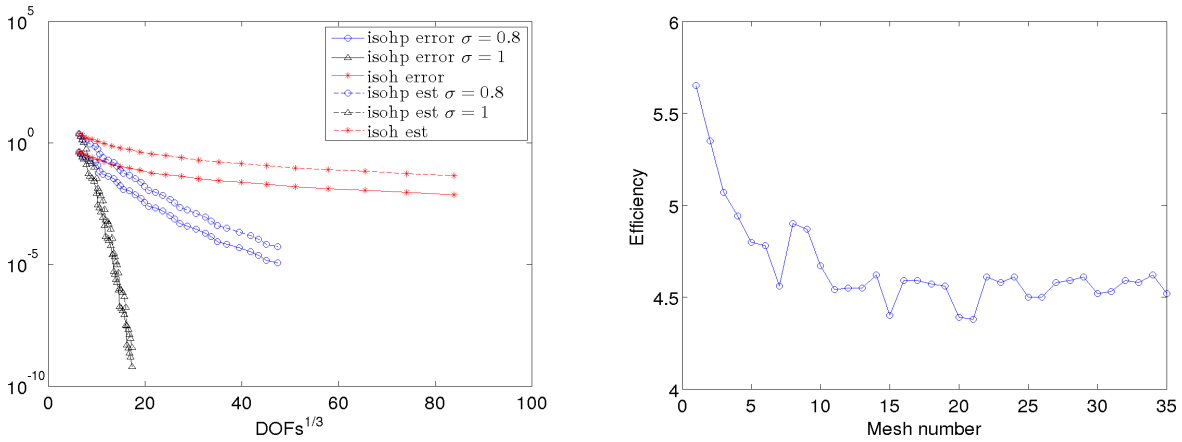

(a) (b)

Figure 2: (a) Convergence results in the DG norm and the error estimator using different refinement techniques for the SP_1 model using $\varepsilon = 1$ and (b) efficiency plot for the isotropic hp-adaptivity technique with $\sigma = 0.8$.

4.2. Example 2

For our second example, we are going to consider a problem with solutions exhibiting boundary layers to test the anisotropic refinement schemes. We first solve the SP_1 problem in an unit squared domain using $\sigma = \kappa = 1$ and $r_1 = r_2 = 0$. The functions F and G in the right-hand side of equations (1) are calculated such that the analytical solution of the SP_1 problem is given by

$$\varphi(x, y) = \left(\frac{e^{\frac{x-1}{A}} - 1}{e^{-\frac{1}{A}} - 1} + x - 1 \right) \left(\frac{e^{\frac{y-1}{A}} - 1}{e^{-\frac{1}{A}} - 1} + y - 1 \right).$$

We solve this problem for two different values of the diffusion scale $\varepsilon = 1.0$ and $\varepsilon = 0.2$. Note that despite the fact that the above exact solution is smooth, it may develop boundary layers along the domain boundary for small values of ε.

In Figure 6 we present the convergence of the errors using different refinement techniques for both values of ε. The adaptive techniques that involve p-refinement perform much better than the others. The formers converge exponentially, as suggested by the plots, instead the remaining only polynomially. Also the techniques with anisotropic refinements converge slightly better than the similar ones but only isotropic, suggesting the advantage of using anisotropic refinement on solution with boundary layers.

In order to assess the accuracy of the error estimator in following the true error, we reported in Figure 7 the comparison between the true errors and the error estimators for the isotropic hp and the anisotropic h isotropic p methods. As can be seen, in all cases the error estimator mimics very well the behaviour of the true error. This is further highlighted

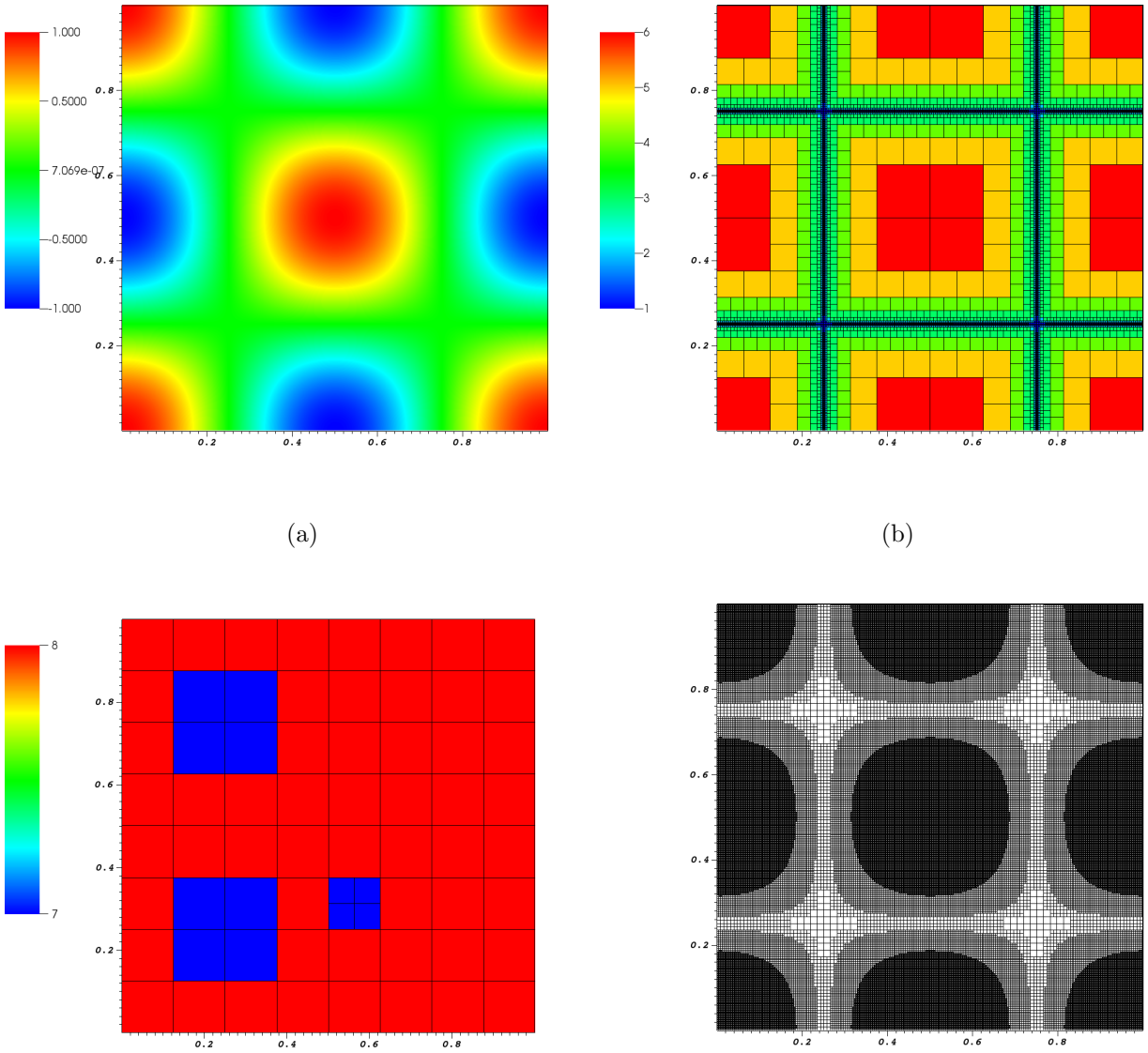

(a) (b)

(c) (d)

Figure 3: (a) Approximation of the solution for the SP_1 model using $\varepsilon = 1$, (b) final isotropiccally hp-adapted mesh with $\sigma = 0.8$, (c) final isotropiccally hp-adapted mesh with $\sigma = 1$ and (d) final isotropiccally h-adapted mesh. The different colours of the elements in the picture on the right rapresent different orders of polynomials.

in Figure 8 by the values of the efficiency indexes that are well bounded for the same two methods.

Before presenting the meshes adapted automatically by the method, we show in Figure

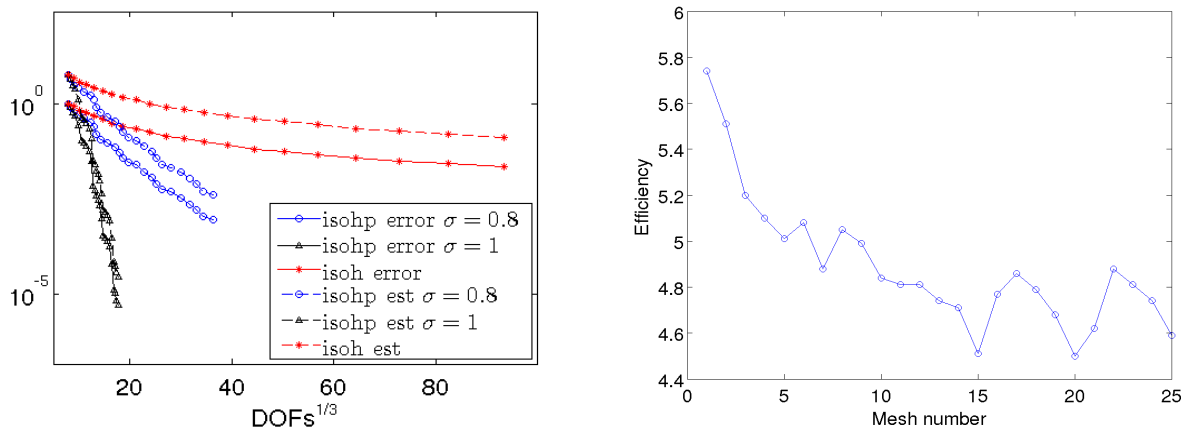

(a) (b)

Figure 4: (a) Convergence results in the DG norm and the error estimator using different refinement techniques for the SP_3 model using $\varepsilon = 1$ and (b) efficiency plot for the isotropic hp-adaptivity technique with $\sigma = 0.8$.

9 the analytical solutions for the SP_1 model using $\varepsilon = 1.0$ and $\varepsilon = 0.2$. Comparing the two images, it is clear the effect of reducing the value of ε on the thickness of the boundary layers on the top and right edges of the domain.

Considering $\varepsilon = 1.0$, Figure 10 shows the final meshes using anisotropic-h isotropic-p and isotropic-hp refinements. Looking along the boundary of the domain, it is clear that the isotropic refinement introduces many more elements resulting in many extra degrees of freedom. However, due to the presence of boundary layers, this does not translate in a better accuracy but, as showed in Figure 6, rather the opposite. Much better performs the anisotropic method that introduces thin and long elements along the edges.

In Figure 11 we have mesh 15 and mesh 35 from the anisotropic-h method for $\varepsilon = 0.2$. As expected by the small value of ε, adaptation is very active along the top and right edges to resolve the strong boundary layer.

Similarly for the SP_3 case, we solve the equations (1) on a unit square using $\sigma = \kappa = 1$, $\alpha_1 = \alpha_2 = \beta_1 = \beta_2 = 1$ and $\mu_1 = \mu_2 = 1$. The right-hand side F and boundary function G in (1) are analytically evaluated such that the exact solution of the SP_3 equations is

$$\begin{aligned}
\psi_1(x,y) &= \left(\frac{e^{\frac{-x}{A_{1,1}}}-1}{e^{-\frac{1}{A_{1,1}}}-1} - x\right)\left(\frac{e^{\frac{-y}{A_{1,1}}}-1}{e^{-\frac{1}{A_{1,1}}}-1} - y\right), \\
\psi_2(x,y) &= \left(\frac{e^{\frac{x-1}{A_{2,2}}}-1}{e^{-\frac{1}{A_{2,2}}}-1} + x - 1\right)\left(\frac{e^{\frac{y-1}{A_{2,2}}}-1}{e^{-\frac{1}{A_{2,2}}}-1} + y - 1\right).
\end{aligned}$$

where $A_{1,1}$ and $A_{2,2}$ are the two diagonal components of A. Note that for this test example, the solution components ψ_1 and ψ_2 present boundary layers respectively, in the upper-right

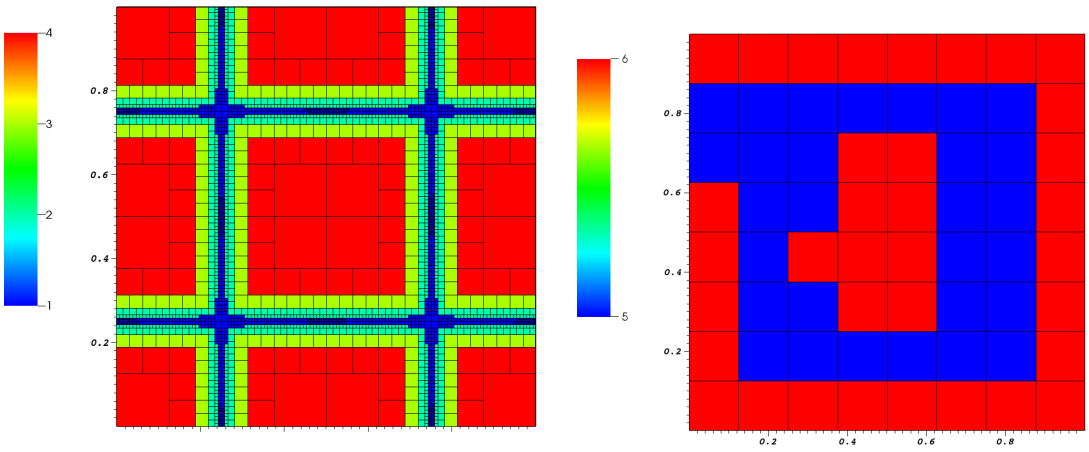

(a) (b)

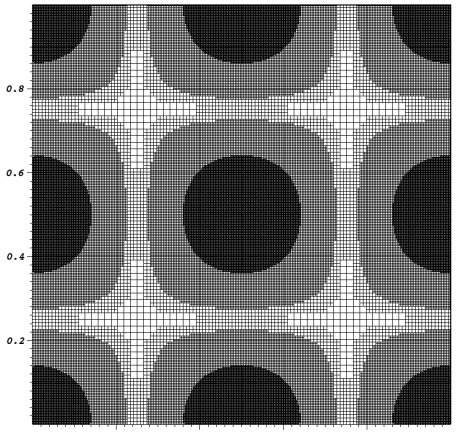

(c)

Figure 5: (a) Final isotropiccally *hp*-adapted mesh for the SP_3 case with $\sigma = 0.8$, (b) final isotropiccally *hp*-adapted mesh with $\sigma = 1$. The different colours of the elements rapresent different orders of polynomials. (c) Final isotropiccally *h*-adapted mesh for the SP_3 case.

and lower-left regions of the computational domain. As in the previous test problem, we consider the two radiative regimes associated with $\varepsilon = 1.0$ and $\varepsilon = 0.2$.

In Figure 12 we present the convergence of the errors using different refinement techniques for both values of ε. The same conclusions as for Figure 6 can also be reached for SP_3. However, one thing that was not present for SP_1 is the fact that for $\varepsilon = 0.2$ we have that at the beginning the anisotropic-*h* refinement is better than the isotropic-*hp*, but after few more meshes the isotropic-*hp* overtakes the anisotropic-*h*. This is because anisotropic-*h*

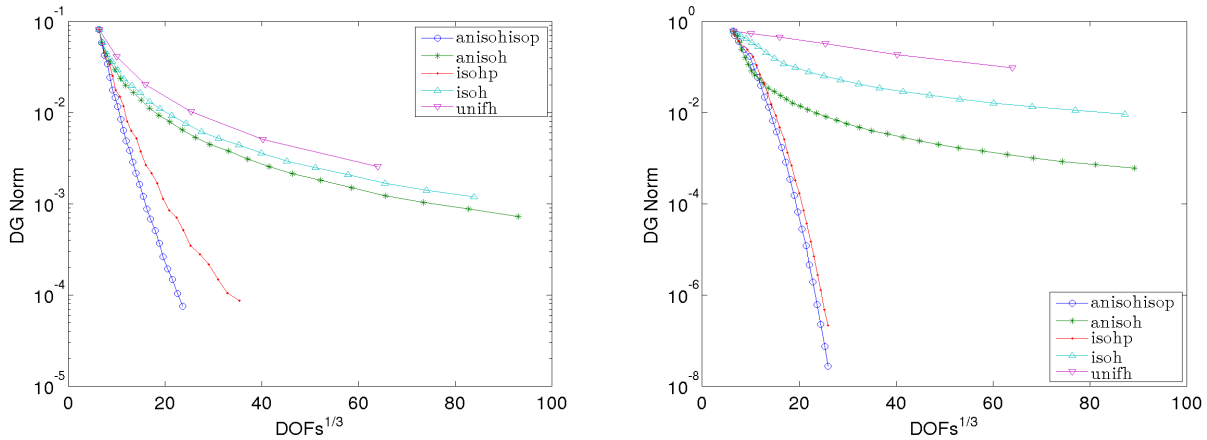

Figure 6: (a) Convergence results in the DG norm using different refinement techniques for the accuracy test problem for the SP_1 model using $\varepsilon = 1.0$ and (b) $\varepsilon = 0.2$.

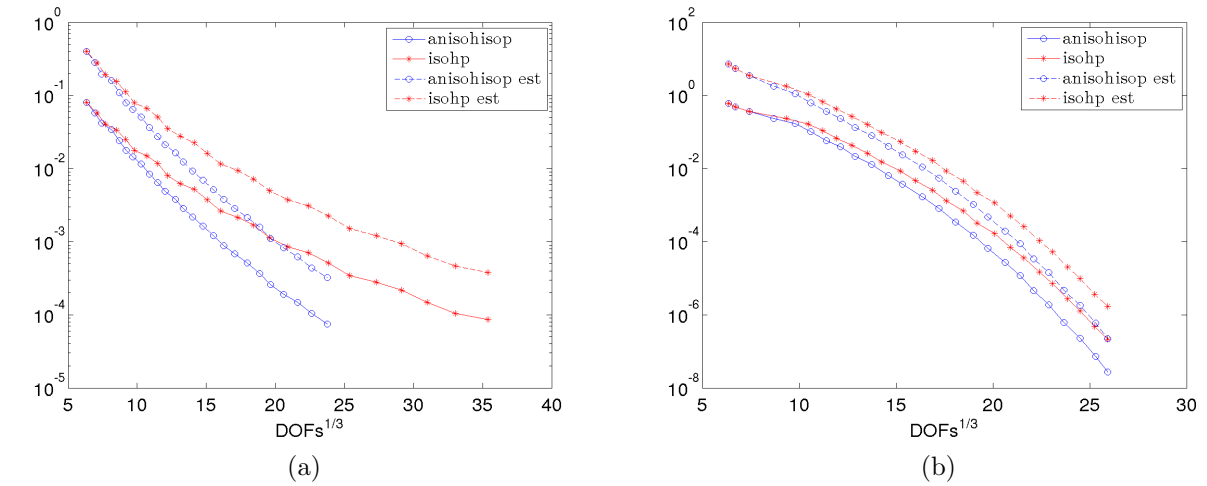

Figure 7: (a) Convergence of the DG norm of the error and the error estimator for the SP_1 model using $\varepsilon = 1.0$ and (b) $\varepsilon = 0.2$.

refinement delivers very quickly an improvement in presence of boundary layers, but since the convergence is only polynomial, due to the lack of p-refinement, it is only a matter of time before the exponentially fast isotropic-hp refinement wins.

In order to assess the accuracy of the error estimator in following the true error for the SP_3 case, we reported in Figure 13 the comparison between the true errors and the error estimators for the isotropic hp and the anisotropic-h isotropic-p methods. As can be seen, in all cases the error estimator mimics very well the behaviour of the true error. This is further

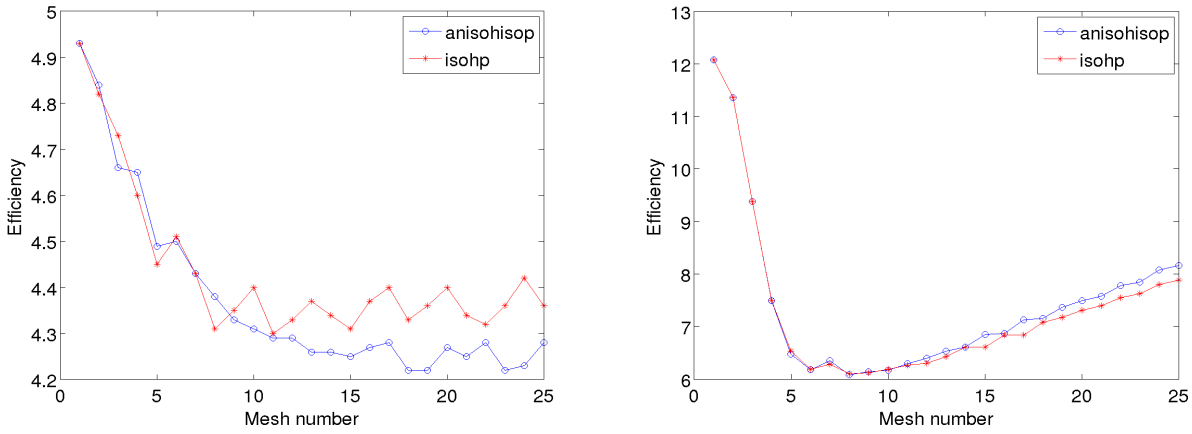

(a) (b)

Figure 8: (a) Efficiency indexes for the SP_1 model using $\varepsilon = 1.0$ and (b) $\varepsilon = 0.2$.

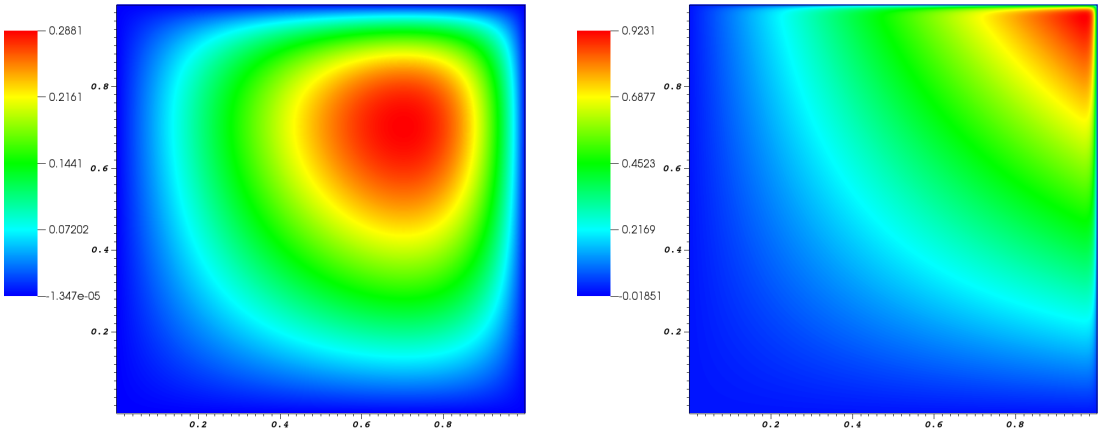

(a) (b)

Figure 9: (a) Solutions for the SP_1 model using $\varepsilon = 1.0$ and (b) $\varepsilon = 0.2$.

highlighted in Figure 14 by the values of the efficiency indexes that are well bounded for the same two methods.

As before, the reduction of the value of ε, makes the boundary layers stronger. This can be appreciated comparing the meshes in Figure 15 and Figure 16.

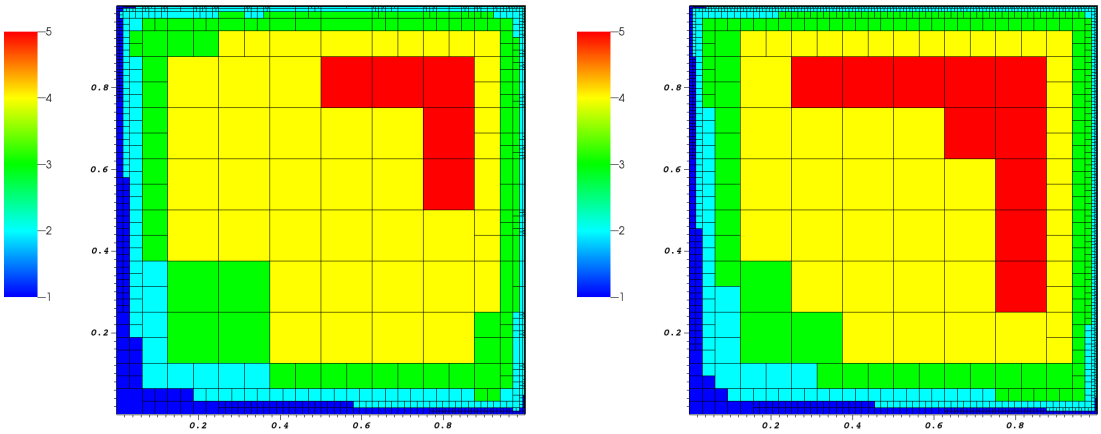

(a) (b)

Figure 10: (a) Final *hp*-adapted meshes for the SP_1 model for $\varepsilon = 1.0$ using anisotropic and (b) isotropic refinement. The different colours of the elements rapresent different orders of polynomials.

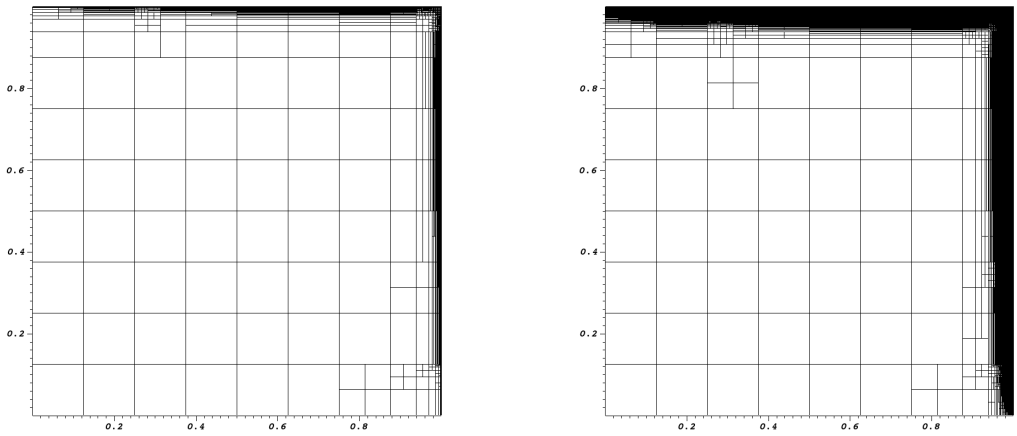

(a) (b)

Figure 11: (a) Anisotropic-*h* adapted meshes for the SP_1 model for $\varepsilon = 0.2$ from iteration number 15 and (b) 35.

5. Conclusions

We have derived a reliable a-posteriori error estimator for DG discretizations of radiative transfer problems on anisotropically refined meshes. We have proved its reliability, up to an

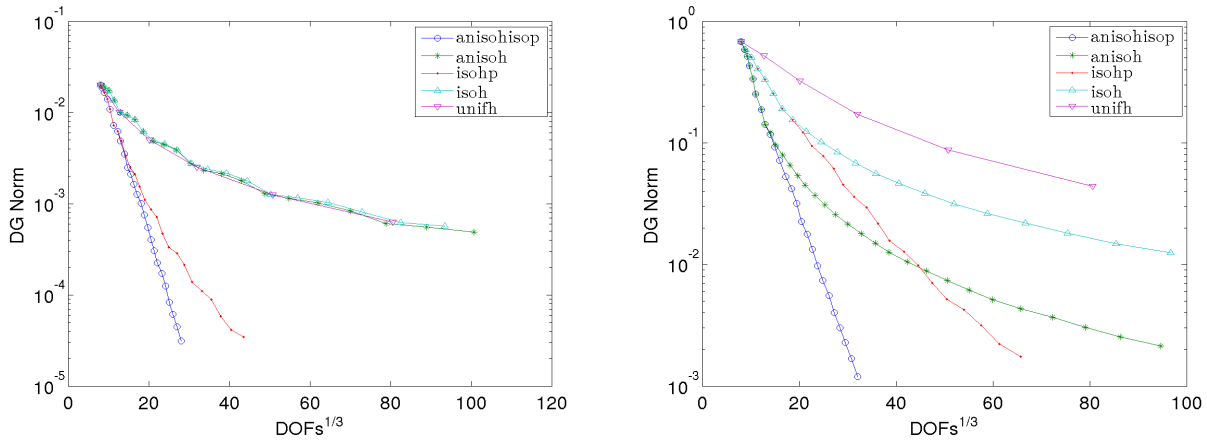

Figure 12: (a)Convergence results in the DG norm using different refinement techniques for the accuracy test problem for the SP_3 model using $\varepsilon = 1.0$ and (b) $\varepsilon = 0.2$.

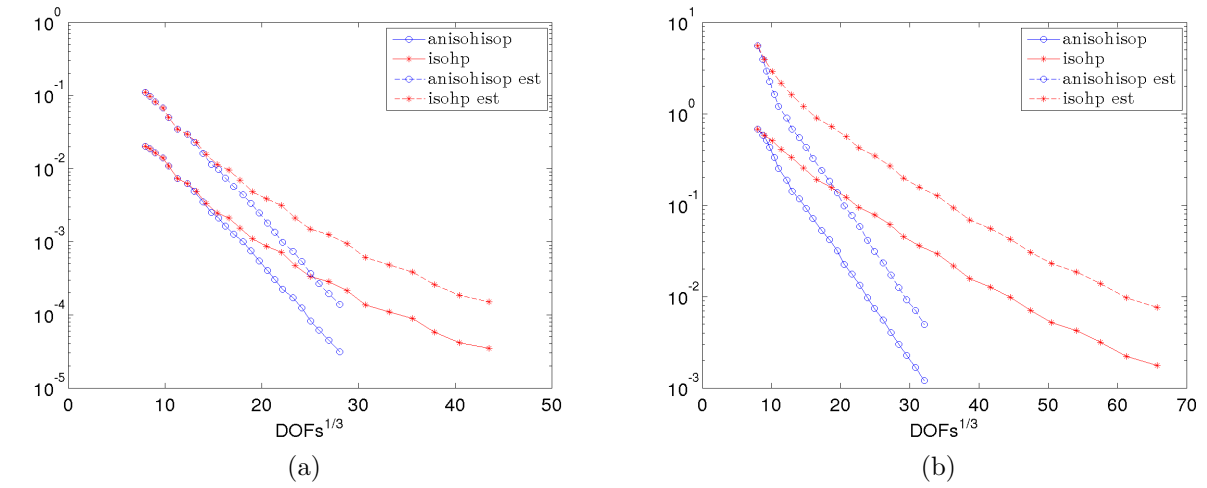

Figure 13: (a) Convergence of the DG norm of the error and the error estimator for the SP_3 model using $\varepsilon = 1.0$ and (b) $\varepsilon = 0.2$.

alignment measure which takes into account the possible anisotropy of the underlying meshes. Our numerical experiments indicate that anisotropic-h isotropic-p adaptive DG method is superior to all other tested strategies converging much faster than all others and delivering high accuracy approximations involving a much smaller number of degrees of freedom. The fact that the method is completely automatic means that it can be used as a black box to solve quickly and accurately radiative transfer problems on a desktop machine also in those cases where the solution presents strong boundary layers.

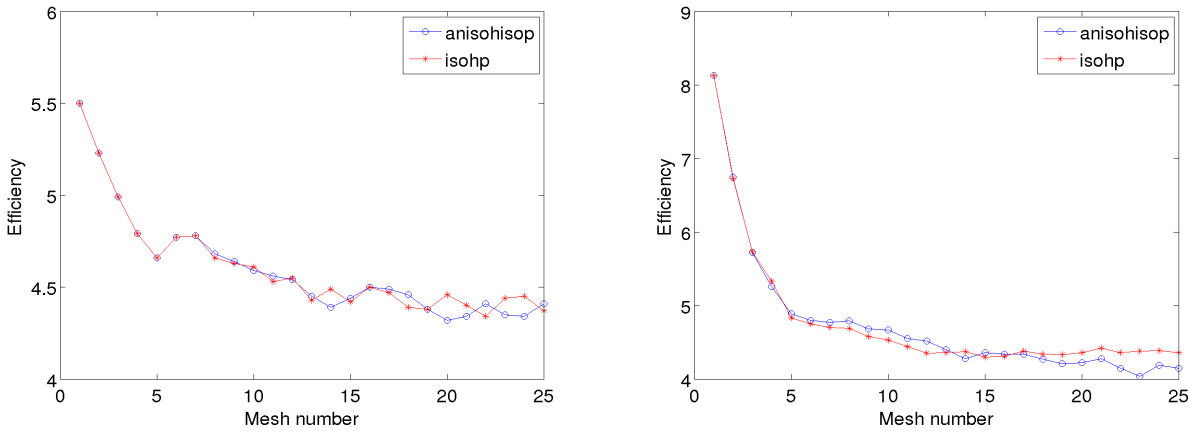

(a) (b)

Figure 14: (a) Efficiency indexes for the SP_3 model using $\varepsilon = 1.0$ and (b)$\varepsilon = 0.2$.

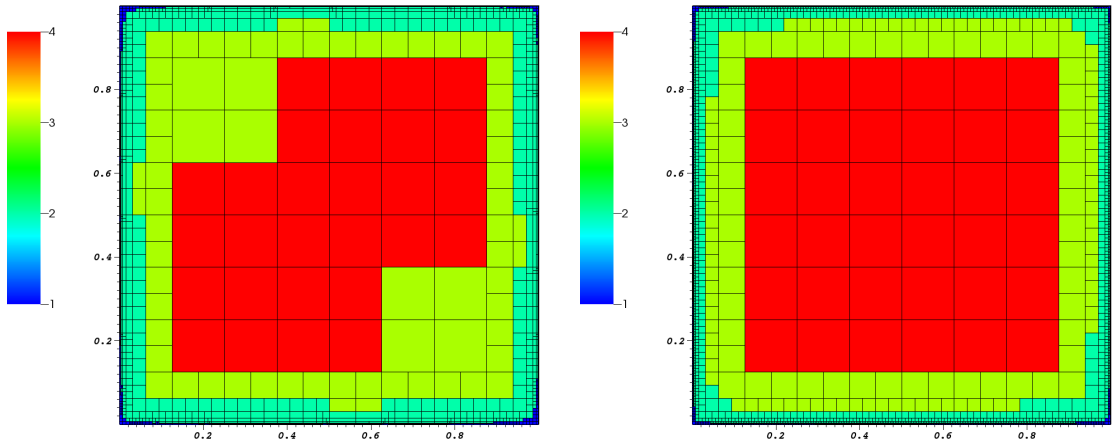

(a) (b)

Figure 15: (a) Final *hp*-adapted meshes for the SP_3 model for $\varepsilon = 1.0$ using anisotropic and (b) isotropic refinement. The different colours of the elements rapresent different orders of polynomials.

[1] S. Giani, M. Seaid, hp-adaptive discontinuous galerkin methods for simplified pn approximations of frequency-dependent radiative transfer, Computer Methods in Applied Mechanics and Engineering 301 (2016) 52–79.

[2] E. Gelbard, Simplified Spherical Harmonics Equations and their Use in Shielding Problems, Technical Report WAPD-T-1182, Bettis Atomic Power Laboratory, 1961.

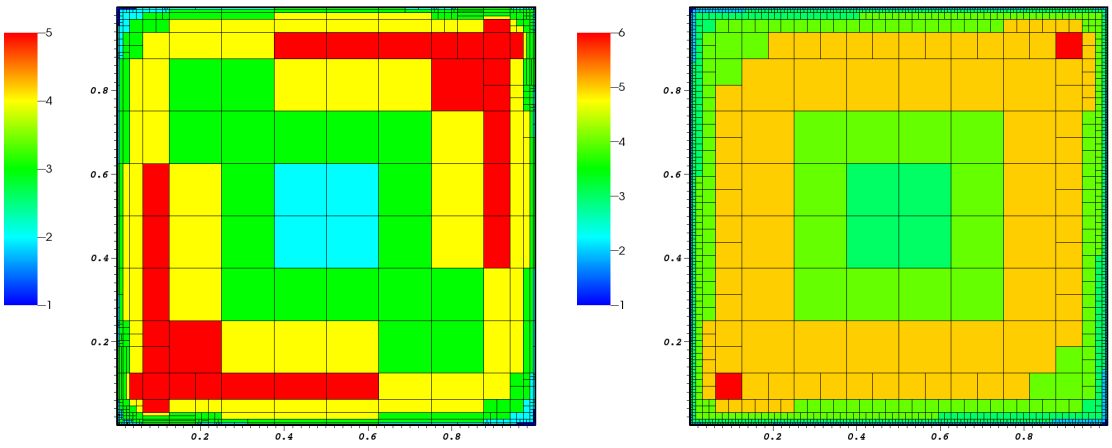

(a) (b)

Figure 16: (a) Final *hp*-adapted meshes for the SP_3 model for $\varepsilon = 1.0$ using anisotropic and (b) isotropic refinement. The different colours of the elements rapresent different orders of polynomials.

[3] E. Larsen, J. Morel, J. McGhee, Asymptotic derivation of the multigroup P_1 and simplified P_N equations with anisotropic scattering, Nucl. Sci. Eng. 123 (1996) 328–367.

[4] E. Larsen, G. Thömmes, A. Klar, M. Seaid, T. Götz, Simplified P_N approximations to the equations of radiative heat transfer and applications, J. Comp. Phys. 183 (2002) 652–675.

[5] G. Thömmes, R. Pinnau, M. Seaid, T. Götz, A. Klar, Numerical methods and optimal control for glass cooling processes, Transp. Theory Stat. Phys. 31 (2002) 513–529.

[6] M. Frank, M. Seaid, J. Janicka, A. Klar, R. Pinnau, G. Thömmes, A comparison of approximate models for radiation in gas turbines, Int. J. Progress in CFD 3 (2004) 191–197.

[7] R. Backofen, T. Bilz, A. Ribalta, A. Voigt, SP_N-approximations of internal radiation in crystal growth of optical materials, J. Crystal Growth. 266 (2004) 264–270.

[8] S. Giani, D. Schötzau, L. Zhu, An a-posteriori error estimate for hp-adaptive DG methods for convection–diffusion problems on anisotropically refined meshes, Computers & Mathematics with Applications 67 (4) (2014) 869–887.

[9] D. Arnold, F. Brezzi, B. Cockburn, L. Marini, Unified analysis of discontinuous Galerkin methods for elliptic problems, SIAM J. Numer. Anal. 39 (2002) 1749–1779.

[10] F. Bassi, S. Rebay, High-order accurate discontinuous finite element solution of the 2D Euler equations, Journal of Computational Physics 138 (2) (1997) 251–285, aCM ID: 274113.

[11] F. Bassi, S. Rebay, A high-order accurate discontinuous finite element method for the numerical solution of the compressible Navier-Stokes equations, J. Comput. Phys. 131 (2) (1997) 267–279.

[12] C. Farhat, I. Harari, U. Hetmaniuk, A discontinuous Galerkin method with Lagrange multipliers for the solution of Helmholtz problems in the mid-frequency regime, Computer Methods in Applied Mechanics and Engineering 192 (2003) 1389–1419.

[13] E. Burman, A. Ern, Continuous Interior Penalty hp-Finite Element Methods for Advection and Advection-Diffusion Equations, Mathematics of Computation 76 (259) (2007) 1119–1140.

[14] A. Buffa, I. Perugia, Discontinuous Galerkin Approximation of the Maxwell Eigenproblem, SIAM Journal on Numerical Analysis 44 (5) (2006) 2198.

[15] G. Kunert, An a-posteriori residual error estimator for the finite element method on anisotropic tetrahedral meshes, Numer. Math. 86 (2000) 471–490.

[16] G. Kunert, A local problem error estimator for anisotropic tetrahedral finite element meshes, SIAM J. Numer. Anal. 39 (2001) 668–689.

[17] L. Formaggia, S. Perotto, Anisotropic error estimates for elliptic problems, Numer. Math. 94 (2003) 67–92.

[18] M. Picasso, An anisotropic error indicator based on Zienkiewicz-Zhu error estimator: Application to elliptic and parabolic problems, SIAM J. Sci. Comput. 24 (2003) 1328–1355.

[19] D. Schötzau, C. Schwab, T. Wihler, *hp*-DGFEM for second-order elliptic problems in polyhedra II: Exponential convergence, submitted 51 (4) (2013) 2005–2035.

[20] E. Georgoulis, E. Hall, P. Houston, Discontinuous Galerkin methods on *hp*-anisotropic meshes I: A priori error analysis, Int. J. Comput. Sci. Math. 1 (2007) 221–244.

[21] E. Georgoulis, E. Hall, P. Houston, Discontinuous Galerkin methods on *hp*-anisotropic meshes II: A-posteriori error analysis and adaptivity, Appl. Numer. Math. 59 (2009) 2179–2194.

[22] S. Prudhomme, F. Pascal, J. Oden, A. Romkes, Review of a priori error estimation for discontinuous Galerkin methods, Tech. Rep. 2000-27, TICAM, University of Texas at Austin (2000).

[23] L. Zhu, S. Giani, P. Houston, D. Schötzau, Energy norm a-posteriori error estimation for *hp*-adaptive discontinuous Galerkin methods for elliptic problems in three dimensions, Math. Models Methods Appl. Sci. 21 (2) (2010) 267–306.

[24] L. Zhu, D. Schötzau, A robust a-posteriori error estimate for *hp*-adaptive DG methods for convection-diffusion equations, IMA J. Numer. Anal. 31 (3) (2011) 971–1005.

[25] L. Zhu, Robust a-posteriori error estimation for discontinuous Galerkin methods for convection-diffusion problems, Ph.D. thesis, University of British Columbia (2010).

[26] P. Houston, D. Schötzau, T. P. Wihler, Energy norm a-posteriori error estimation of *hp*-adaptive discontinuous Galerkin methods for elliptic problems, Math. Models Methods Appl. Sci. 17 (2007) 33–62.

[27] D. Schötzau, L. Zhu, A robust a-posteriori error estimator for discontinuous Galerkin methods for convection-diffusion equations, Appl. Numer. Math. 59 (2009) 2236–2255.

[28] P. R. Amestoy, I. S. Duff, J. Koster, J.-Y. L'Excellent, A fully asynchronous multifrontal solver using distributed dynamic scheduling, SIAM Journal on Matrix Analysis and Applications 23 (2001) 15–41.

[29] P. R. Amestoy, I. S. Duff, J.-Y. L'Excellent, Multifrontal parallel distributed symmetric and unsymmetric solvers, Comput. Methods Appl. Mech. Eng. 184 (2000) 501–520.

[30] P. R. Amestoy, A. Guermouche, J.-Y. L'Excellent, S. Pralet, Hybrid scheduling for the parallel solution of linear systems, Parallel Computing 32 (2006) 136–156.

[31] P. Houston, E. Süli, Adaptive finite element approximation of hyperbolic problems, in: T. Barth, H. Deconinck (Eds.), Error Estimation and Adaptive Discretization Methods in Computational Fluid Dynamics. Lect. Notes Comput. Sci. Engrg., Vol. 25, Springer–Verlag, 2002, pp. 269–344.

[32] P. Houston, E. Süli, A note on the design of *hp*–adaptive finite element methods for elliptic partial differential equations, Comput. Methods Appl. Mech. Engrg. 194 (2005) 229–243.